Mutual Intrusion of a Gravity Current and Density Front Formation

DONG-PING WANG

Energy and Environmental Systems Division, Argonne National Laboratory, Argonne, IL 60439

ABSTRACT

A two-dimensional prognostic model was employed to examine the mutual intrusion of a gravity current and the formation of a density front. The results indicated strong vertical motion near the front and, with Earth rotation included, a baroclinic alongshore jet. Comparison with observations from the New England shelf–slope front indicated that the model gives a realistic description of the frontal structure and the mean southward current.

1. Introduction

In coastal oceanic regions, two water masses are usually separated by a density front, i.e., a narrow zone of sharp density gradient. For example, in estuaries, a bottom salinity front (salt wedge) separates the incoming ocean water from the estuarine water. Near the river mouth, a surface salinity front (river plume) separates the spreading, brackish water from the ocean water. On shallow continental shelves, fronts are formed at the transition between well-mixed and stratified water (Simpson *et al.*, 1978). And along the shelf break, a semi-permanent shelf–slope front is formed during the winter months, separating cold, fresh shelf water from warm, saline open-ocean water (Allen *et al.*, 1983). A similar type of the density front is formed at the ice edge (Muench, 1983).

In general, when two fluids are mixed, there will be a smooth transition of density difference. Hence, in order to maintain a sharp density gradient, the advection of a density field must overcome diffusion. For a river plume, Kao *et al.* (1977) showed that at the head of a gravity current, the front is formed by the intense sinking of fresh surface water. Their results are consistent with the observation that the frontal zone forms a strong surface convergence. The model prediction also agreed quantitatively with data from the Connecticut River plume (Garvine and Monk, 1974).

In a river plume, the buoyancy difference is generated by a constant flux of the river water. In general, in coastal waters, the buoyancy difference may also be generated by differential advection and differential mixing. For example, in estuaries, during ebb tide the differential advection of low-salinity water between the coastal and open water area can generate a strong cross-channel salinity gradient (Sick *et al.*, 1978). The differential vertical mixing in shallow seas, caused by the variations of tidal currents, can also generate a strong

horizontal density gradient during summer months (Simpson *et al.*, 1978).

Csanady (1971, 1978b) studied the equilibrium state of a density front resulting from the geostrophic adjustment between two initially separated water masses. The initial buoyancy difference presumably is caused by the differential mixing between nearshore and open water. By using a two-layered model, Csanady demonstrated the formation of a wedge-shaped density front. Hsueh and Cushman-Roisin (1983) and Ou (1983) extended Csanady's model to include a sloping bottom. While these studies revealed the dynamics of geostrophic adjustment, the model predicted an unrealistically large undercurrent in the lower layer. Furthermore, the two-layered model does not allow mixing between the two water masses; hence the model does not predict the cross-frontal circulation. James (1978) indicated that the undercurrent can be reduced by friction; however, his model does not predict the density change.

In this paper, using a two-dimensional prognostic model, we examined the flow adjustment between two initially separated water masses. We studied both rotating and nonrotating cases. The model is also applied to simulate the New England shelf–slope front.

2. Model description

We considered a two-dimensional balance in a vertical plane across the density front. The equations of motion can be derived as a special case of the island shelf circulation model (Wang, 1982) by letting tangential gradients equal zero (e.g., see Hamilton and Rattray, 1978). In Cartesian coordinates:

$$\frac{\partial u}{\partial t} + \frac{\partial}{\partial x}(uu) + \frac{\partial}{\partial z}(uw) - fv$$
$$= -\frac{1}{\rho_0}\frac{\partial P}{\partial x} + \frac{\partial}{\partial z}\left(A_V\frac{\partial u}{\partial z}\right) + A_H\frac{\partial^2 u}{\partial x^2}, \quad (1)$$

$$\frac{\partial v}{\partial t} + \frac{\partial}{\partial x}(uv) + \frac{\partial}{\partial z}(vw) + fu = \frac{\partial}{\partial z}\left(A_V \frac{\partial v}{\partial z}\right) + A_H \frac{\partial^2 v}{\partial x^2},$$

$$\tag{2}$$

$$-\frac{\partial P}{\partial z} = \rho g, \tag{3}$$

$$\frac{\partial S}{\partial t} + \frac{\partial}{\partial x}(uS) + \frac{\partial}{\partial z}(wS) = \frac{\partial}{\partial z}\left(K_V \frac{\partial S}{\partial z}\right) + K_H \frac{\partial^2 S}{\partial x^2},$$

$$\tag{4}$$

$$\frac{\partial u}{\partial x} + \frac{\partial w}{\partial z} = 0, \tag{5}$$

$$\rho = \rho_0 + \beta S, \tag{6}$$

where u, v, w, are respective offshore, alongshore and vertical velocities, S is the salinity, f the Coriolis parameter, P the pressure, ρ the density, ρ_0 a reference density, A_V and A_H are the vertical and horizontal viscosity coefficients, and K_V and K_H the corresponding diffusivity coefficients. In Eqs. (1)–(5), we assumed that motion is hydrostatic and water is incompressible. The boundary conditions are:

1) At the sea surface there is no surface stress;

$$A_v\left(\frac{\partial u}{\partial z}, \frac{\partial v}{\partial z}\right) = 0, \tag{7a}$$

$$K_v \frac{\partial S}{\partial z} = 0. \tag{7b}$$

2) At the ocean bottom there is bottom friction:

$$A_v\left(\frac{\partial u}{\partial z}, \frac{\partial v}{\partial z}\right) = -\lambda(u, v), \tag{8}$$

where λ is a linear drag coefficient.

3) At the coast the normal flow vanishes;

$$u = 0, \tag{9a}$$

$$A_H\left(\frac{\partial u}{\partial x}, \frac{\partial v}{\partial x}\right) = 0, \tag{9b}$$

$$K_H \frac{\partial S}{\partial x} = 0. \tag{9c}$$

4) At the open-ocean end, the ambient conditions are specified as

$$\eta = 0, \tag{10a}$$

$$S = S_0(z), \tag{10b}$$

where η is the free surface and S_0 is the ambient salinity profile. In the model application, the open-ocean end is placed far from the region of the density adjustment so that the open boundary condition is inconsequential.

The vertical eddy coefficients are the Munk-Anderson type (cm^2 s^{-1}):

$$A_v = A_v^0(1 + 10 \text{ Ri})^{-1/2}, \tag{11a}$$

$$K_v = K_v^0(1 + 3.33 \text{ Ri})^{-3/2}, \tag{11b}$$

where Ri is the local Richardson number,

$$\text{Ri} = -\frac{g}{\rho_0}\frac{\partial \rho}{\partial z}\left[\left(\frac{\partial u}{\partial z}\right)^2 + \left(\frac{\partial v}{\partial z}\right)^2\right]^{-1/2}. \tag{12}$$

The horizontal eddy coefficients are (cm^2 s^{-1})

$$A_H = 10^5, \tag{13a}$$

$$K_H = 10^5. \tag{13b}$$

The small horizontal diffusion has no effect on the motion. The initial condition is

$$\left.\begin{array}{ll} S = S_1, & x \leq x_0 \\ S = S_2, & x > x_0 \end{array}\right\}. \tag{14}$$

In other words, the two homogeneous water masses are initially separated by a vertical barrier located at $x = x_0$. The density difference between the two water masses, $\Delta\rho = \rho_2 - \rho_1$, is $0.5\sigma_t$ (0.5×10^{-3} g cm^{-3}).

The solution technique for Eqs. (1)–(14) follows the numerical procedure for the island shelf circulation model (Wang, 1982). In essence, Eqs. (1)–(5) are written in staggered-grid, centered-difference form and are solved with a leapfrog scheme in time, except for the advection terms in the salinity equation which are solved with an upwind scheme. The model uses a mode-split technique in the vertical direction and a semi-implicit scheme in the horizontal direction to achieve computational efficiency.

Our model formulation is different from that of Kao et al. (1977) and Kao (1981). In this study, we solved the primitive equations directly together with the complete boundary conditions. Kao et al., on the other hand, reduced the primitive equations to a stream-function form; consequently, it is more convenient in their studies to assume that the ocean surface and the ocean bottom are streamlines. Also, because Kao et al. were interested in the surface plume problem, they did not examine the effects of bottom slope.

3. Results

a. Nonrotating case

We first studied the case of no Earth rotation, i.e., $f = 0$. This case is also equivalent to the problem of two-dimensional estuarine circulation in a narrow channel with cross-channel velocity $v = 0$ (Wang and Kravitz, 1980). For a flat bottom, we chose water depth $H = 50$ m, $\lambda = 0.01$ cm s^{-1}, and $A_v^0 = K_v^0 = 5$ cm^2 s^{-1}. The vertical barrier, which is located 16 km offshore, is opened instantaneously at $t = 0$. The density (salinity) and flow field at $t = 10$ and 20 h are shown in Figs. 1a, b. A sharp front is formed between the two water masses. The front stretches out from the initial vertical line of separation at a constant speed
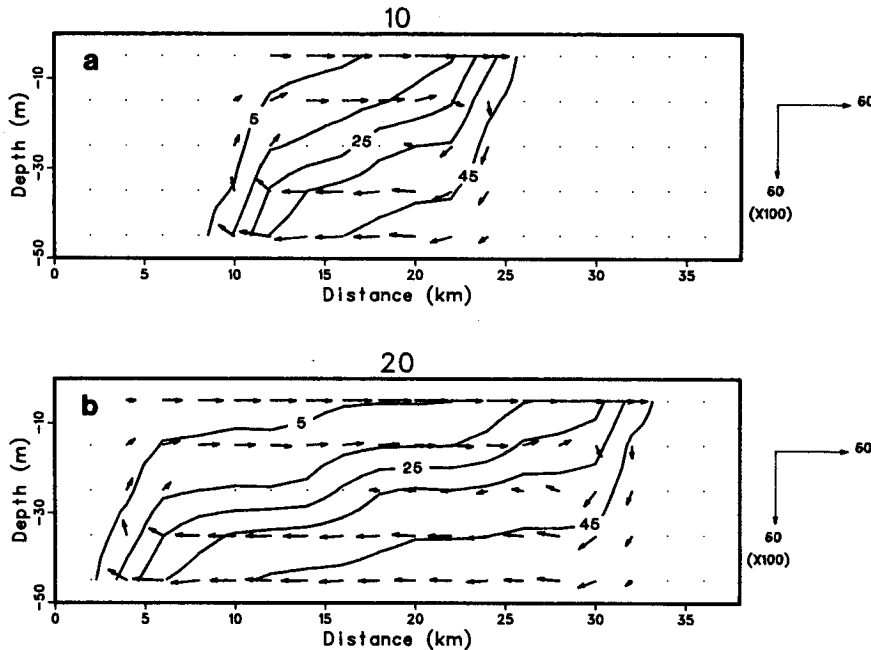
FIG. 1. The cross-frontal circulation (cm s^{-1}) and density (0.01σ_t) at (a) 10 h and (b) 20 h, for $A_v^o = K_v^o = 5$ cm^2 s^{-1}.

of $\sim$24 cm s^{-1} at the surface and 20 cm s^{-1} at the bottom. The slower bottom frontal velocity is caused by friction. The phase speed of the internal gravity wave, which is a reference velocity, is $(gH\Delta\rho/\rho_0)^{1/2}$ = 50 cm s^{-1}. Thus, the front moves at about half of the gravity wave speed. This result also can be deduced from the energy consideration. The total potential energy (per unit volume) at $t = 0$, is $\frac{1}{2}gH(\rho_1 + \rho_2)$. Assuming no mixing between the two waters, behind the front, the density structure must be a layer of lighter water (ρ_1) overlaying a layer of heavier water (ρ_2) of equal thickness. The potential energy of the transient state is $\frac{3}{4}gH\rho_1 + \frac{1}{4}gH\rho_2$. From the energy conservation, the net change of potential energy, $\frac{1}{4}gH\Delta\rho H$, must be equal to the total kinetic energy, $\rho_0 U_f^2$. Or, $U_f = \frac{1}{2}(gH\Delta\rho/\rho_0)^{1/2}$.

The velocity distribution (Fig. 1) shows a strong recirculation, with sinking at the head of the surface front and rising at the head of the bottom front. Maximum horizontal velocity is about 40 cm s^{-1} at the surface and 30 cm s^{-1} at the bottom. The ratio between the maximum surface velocity and the frontal velocity is 1.6. Thus, when an observer travels with the surface front, water will appear to converge from both sides of the front. The maximum vertical velocity is about 0.1 cm s^{-1}.

The flow adjustment is modified by viscous effects. The viscous drag becomes important when thickness of the shear layer, $\delta \sim (A_v t)^{1/2}$, is comparable to the thickness of the front (Huppert, 1982). Eventually, a steady-state balance will be achieved between the ver-

tical viscosity and the density gradient. For $A_v^o = K_v^o$ = 50 cm^2 s^{-1}, the transition time,

$$t_1 \sim \frac{1}{A_v}\left(\frac{H}{2}\right)^2,$$

is about 30 h. The velocity and density at $t = 10$ and 20 h are shown in Figs. 2a, b. The initial spreading of the density front is not affected by the viscosity. However, the propagation of front is slowed down considerably at $t = 20$ h. The vertical shears also are affected by the viscosity; for example, the maximum velocity shear which is located behind the surface front, is 2.9 $\times$ 10^{-2} s^{-1} for small viscosity and it is 1.2 $\times$ 10^{-2} s^{-1} for large viscosity.

When the vertical line of density separation is initially located on a sloping bottom ($x_0 = 16$ km), the flow adjustment will be affected by the downslope gravitational acceleration. For the case of a constant bottom slope and $A_v^o = K_v^o = 50$ cm^2 s^{-1}, the velocity and density distribution at $t = 10$ and 20 h are shown in Figs. 3a, b. The propagation of surface front into the deep water is the same as in the shallow, flat-bottom case. However, at the head of the front there is a strong, local recirculation resulting in an outcropping of the isopycnals. The same features also are found in Kao *et al.* (1977) for the surface plume. Indeed, as the surface front leaves the bottom, it behaves like a shallow, surface plume. On the other hand, shoreward propagation of the bottom front is restrained by the opposing, downslope gravitational acceleration. Because heavier water can barely intrude onto the
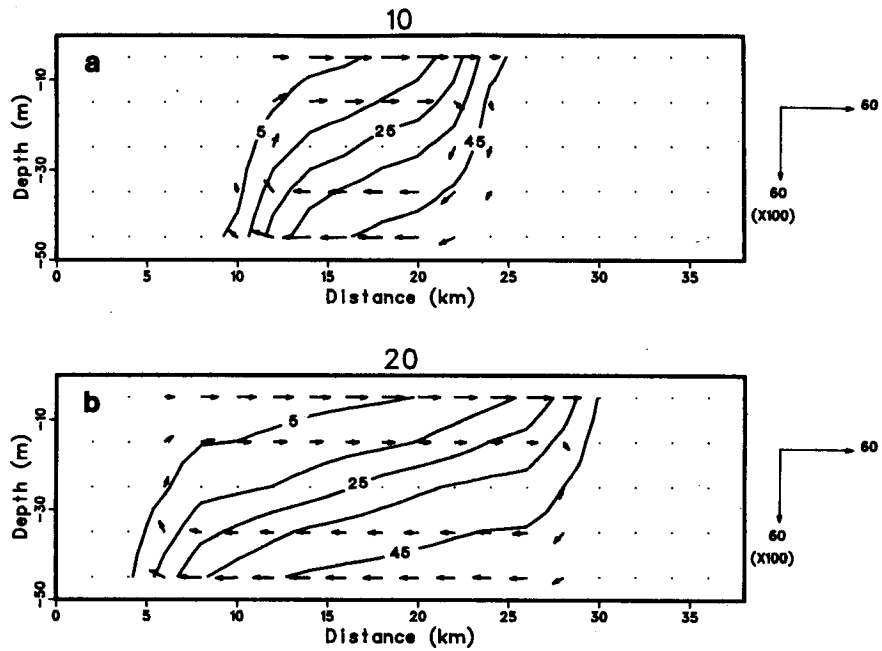
FIG. 2. As in Fig. 1 but for $A_v^o = K_v^o = 50$ cm^2 s^{-1}.
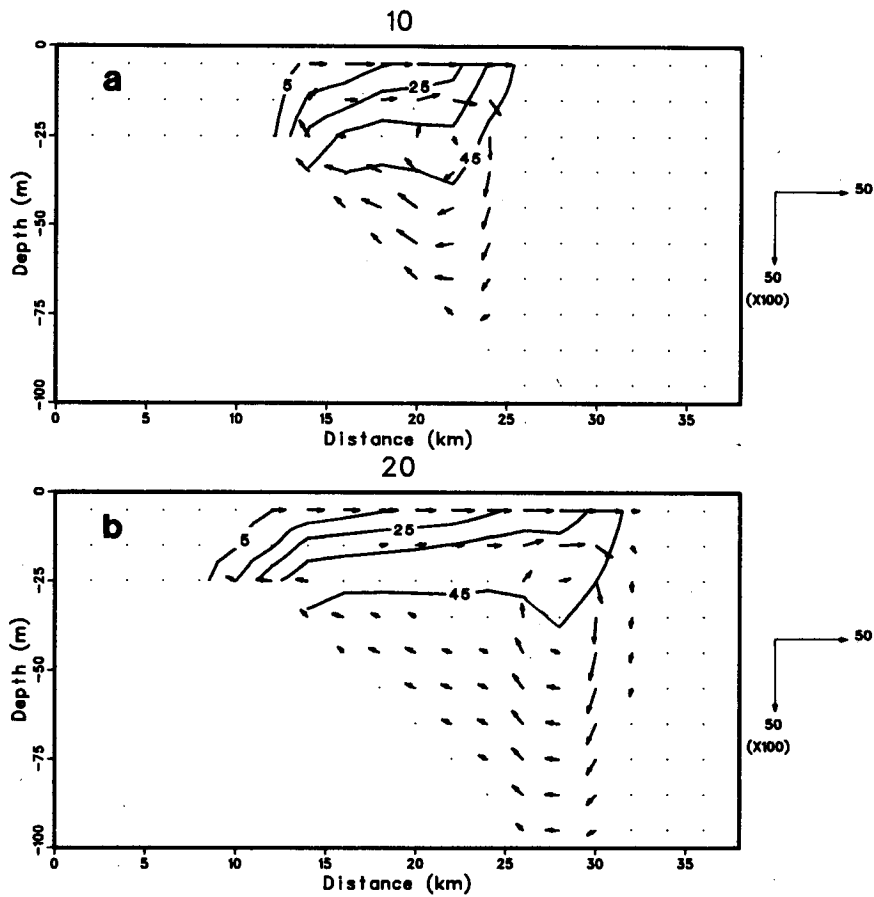

FIG. 3. As in Fig. 2 but for the sloping bottom case.

shallow region, a stationary front is formed at the shelf break.

b. Rotating case

When the channel width in estuaries or the frontal length in open waters is significantly less than the baroclinic radius of deformation, the effect of Earth rotation may be neglected. Otherwise, the Earth rotation must be considered in the study of flow adjustment. We chose $f = 0.93 \times 10^{-4}$ s^{-1} corresponding to 40°N. For $H = 50$ m and $\Delta\rho = 0.5\sigma_t$, the radius of deformation, $R_D = (gH\Delta\rho/\rho)^{1/2} f^{-1}$, is about 5 km, comparable to the frontal length scale studied in the previous section. Hence, the previous results are valid only for narrow channels or short periods. In this section, we reexamine the flow adjustment when Earth rotation is included.

For a constant water depth, $H = 50$ m, and $\lambda = 0.01$ cm s^{-1} and $A_v^o = K_v^o = 5$ cm^2 s^{-1}, the surface cross- and alongshore velocities during the first 40 h after the vertical barrier is opened, are shown in Figs. 4a, b. Without rotation, the surface front moves at about 24 cm s^{-1} toward the open water, the cross-shore velocity is positive, and the alongshore velocity is zero (Figs. 1a, b). With rotation, the front stays near the initial position ($x_0 = 16$ km), and the surface velocities go through a sequence of oscillations with decaying amplitude. The period of oscillation is about 19 h, and the two velocity components are 90° out-of-phase. In other words, during the initial adjustment, the flow is dominated by an inertial oscillation. Kao (1981) also found large inertial oscillations in the plume model when Earth rotation is included.

The inertial motion, which is damped rapidly by friction, has an amplitude of less than 1 cm s^{-1} after 5 cycles. On the other hand, the mean cross-shore circulation also is quite small, on the order of 1 cm s^{-1}. Thus, the distinction between mean and fluctuating components may not be obvious. This problem can be resolved by using a larger viscosity which damps inertial oscillation more rapidly while having little effect on the mean circulation. In subsequent studies, we chose $A_v^o = K_v^o = 50$ cm s^{-1}. A larger viscosity probably is more realistic for coastal application (Hamilton and Rattray, 1978).

Figures 5a, b show the density and velocity at $t = 120$ h for $A_v^o = K_v^o = 50$ cm^2 s^{-1}; the inertial oscillation is completely removed after 6 inertial periods. The density front is about 15 km wide, i.e., about $3R_D$, centered about the initial position ($x_0 = 16$ km). On the cross-frontal plane, a recirculation pattern is evident, though its magnitude is much smaller than the corresponding nonrotating case (Fig. 2). The maximum cross-shore velocity is about 1 cm s^{-1}, compared with 20 cm s^{-1} in the nonrotating case. The maximum vertical velocity is about 10^{-3} cm s^{-1}. On the other hand, a strong surface jet is formed along the front with a maximum amplitude of 10 cm s^{-1} (Fig. 5b).
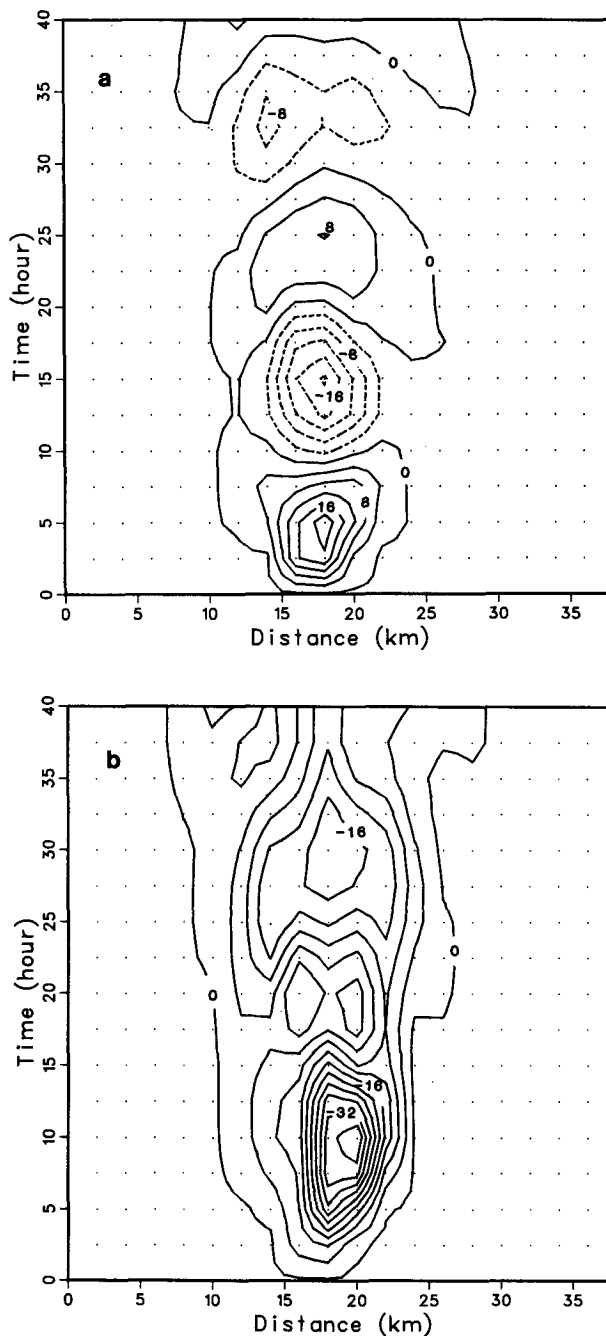

Fig. 4. The surface velocities (cm s^{-1}) during the initial adjustment: (a) cross-shore velocity and (b) alongshore velocity.

The direction of the jet is such that facing downstream, the lighter water is on the right. On the east coast of a continent, the alongshore current moves toward the equator. The alongshore current speed decreases with depth with a slight flow reversal (about 2 cm s^{-1}) near the bottom. For comparison, the two-layered, frictionless model (Csanady, 1978b) predicts a maximum current of about 40 cm s^{-1} in each layer with opposite directions.
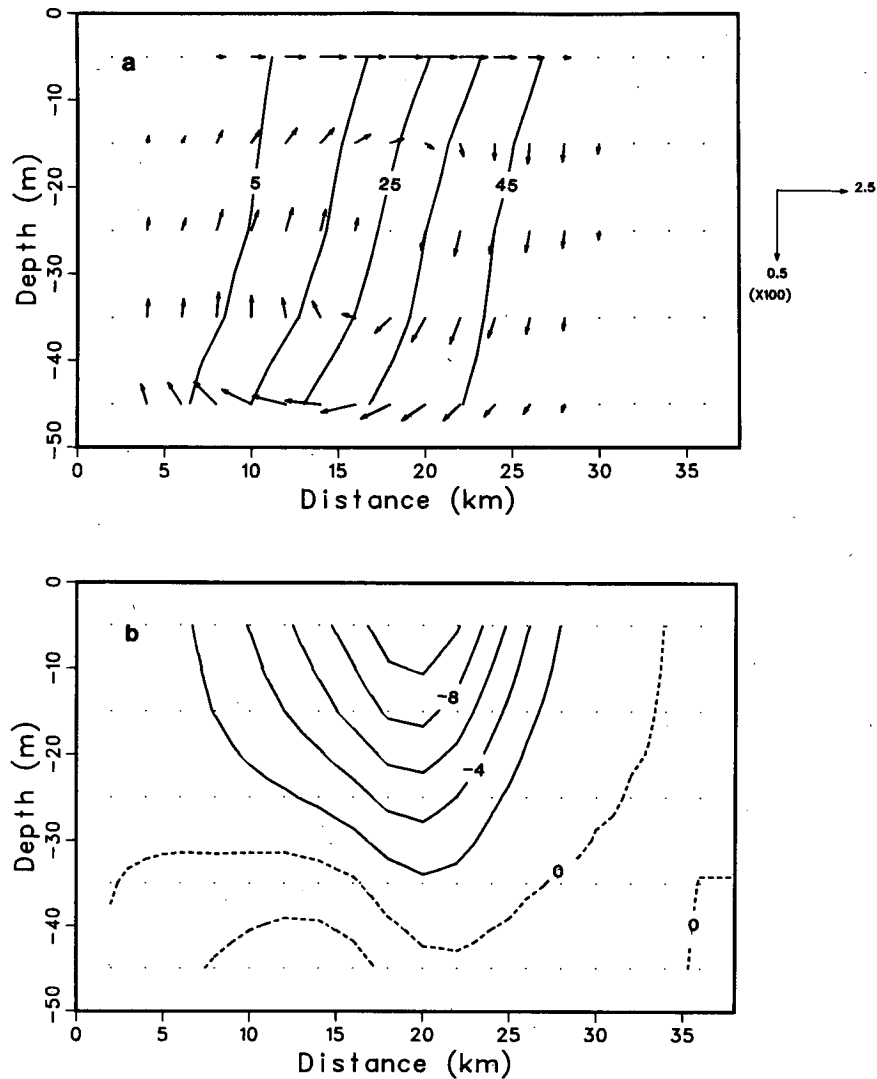
FIG. 5. The steady-state frontal structure for the flat bottom case: (a) the cross-shore circulation
(cm s^{-1}) and density (0.01σ_t), and (b) the alongshore velocity (cm s^{-1}).

The difference between the nonrotating and the rotating case indicates that the dynamical balance for flow adjustment is altered by the effect of Earth rotation. In the nonrotating case, the density difference is balanced by advection of cross-shore momentum. With rotation, the density difference is in geostrophic balance with an alongshore current. The cross-shore velocity is induced by the vertical velocity shear. The lower-layer jet found in the frictionless model no longer exists because of bottom dissipation.

When the vertical line of separation is located on a sloping bottom, the resulting density front tends to tilt much farther offshore than in the constant depth case (Fig. 6a). Nevertheless, the steady-state flow pattern is similar to that of the constant depth case. The flow is offshore at the surface and onshore near the bottom. In the alongshore direction, a surface jet is located at

the shelf break (Fig. 6b). Because geostrophy dominates the cross-frontal momentum balance, the downslope gravitational acceleration has a less profound effect on the flow adjustment than in the corresponding nonrotating case.

4. Application to the shelf–slope front

Around the Georges Bank and along the Middle Atlantic Bight, a semipermanent shelf–slope front separates the less-saline shelf water from the more-saline slope water (Allen et al., 1983). On the Georges Bank strong tidal currents keep the shelf water well-mixed throughout the year and the cross-shore density difference is stronger during summer when the shelf water is warmer than the slope water. In the Middle Atlantic Bight the cross-shore density is about the same through
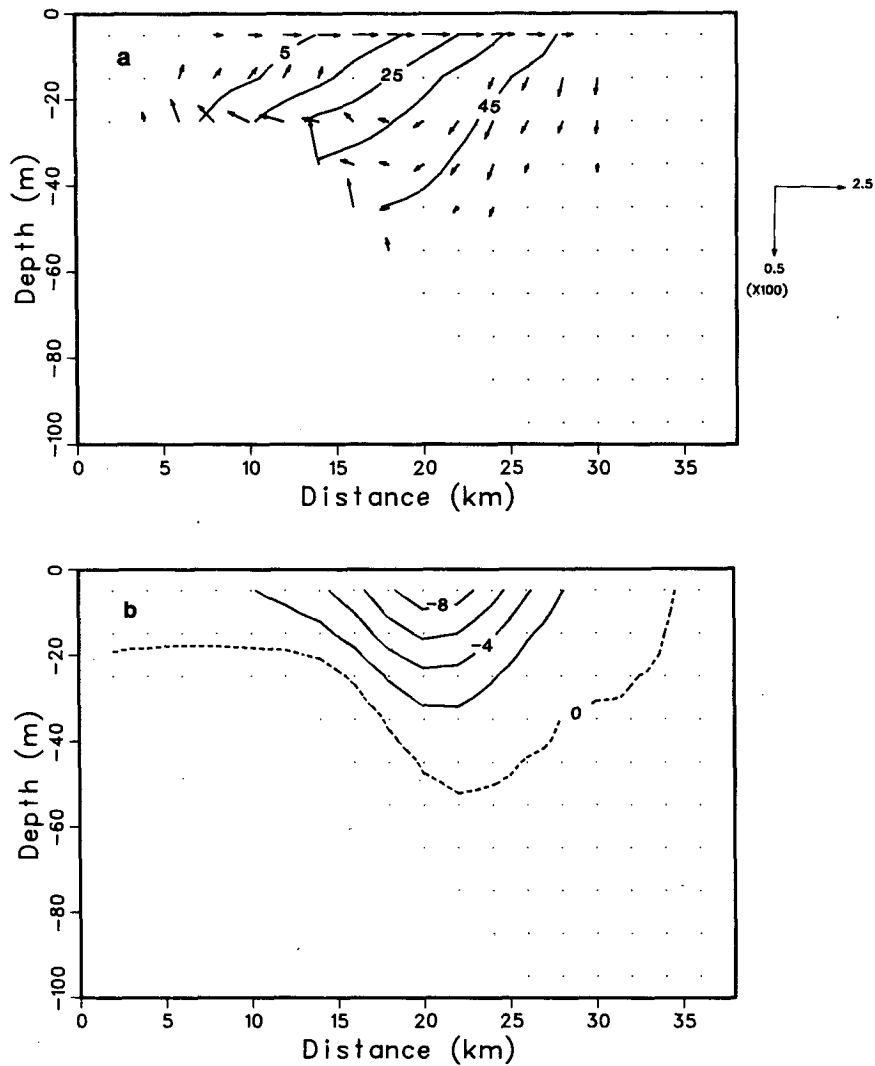
FIG. 6. As in Fig. 5 but for the sloping-bottom case.

the year; though the density front is sharper in winter when the shelf water is well-mixed. Associated with the shelf–slope front is a sheared, longshore geostrophic current or "jet". The jet is southward on the Middle Atlantic Bight, and it forms a clockwise gyre around the Georges Bank. In both cases, the direction of the jet is such that, facing downstream, lighter water is on the right.

To investigate the shelf–slope front, the effect of temperature, as well as salinity, on density must be considered. The conservation equation for temperature is added to the equations of motion, Eqs. (1)–(5),

$$\frac{\partial T}{\partial t} + \frac{\partial}{\partial x}(uT) + \frac{\partial}{\partial z}(wT) = \frac{\partial}{\partial z}\left(K_v \frac{\partial T}{\partial z}\right) + K_H \frac{\partial^2 T}{\partial x^2},$$
(15)

where T is the temperature. The equation of state (6)

is also replaced by a more complete state equation (Mamayev, 1975):

$$\sigma_t = 28.152 - 0.0735T - 0.00469T^2$$

$$+ (0.802 - 0.002T)(S\text{-}35),$$
(16)

$$\rho = 1 + \sigma_t \times 10^3,$$
(17)

where, T is in units of °C, S in ‰ and ρ in g cm^{-3}.

We considered the case of the wintertime New England shelf–slope front. The water masses are formed by mixing two water types: cold and fresh shelf water ($T = 6$°C, $S = 33$‰, $\sigma_t = 26.0$) and warm and more-saline slope water ($T = 12.5$°C, $S = 35$‰, $\sigma_t = 26.5$). We assumed that the two homogeneous waters are initially separated at the shelf break ($x_0 = 0$ km, water depth = 80 m) due to the differential mixing between shelf and slope region. The steady-state temperature (salinity), cross-shore circulation and alongshore cur-

rent are shown in Figs. 7a–c. In the model simulation, we chose $A_v^\circ = K_v^\circ = 50$ cm^2 s^{-1} and $\lambda = 0.1$ cm s^{-1}. Because of the large bottom drag coefficient, the alongshore current is subject to strong dissipation. The alongshore transport will reach a steady state only when the bottom alongshore velocity is identical to zero. In the model simulation, the bottom alongshore velocity is less than 0.05 cm s^{-1} after 600 h. While the velocity is still gradually decreasing, the solution at 600 h is a practical choice for the equilibrium state.

The temperature distribution (Fig. 7a) indicates a sharp front at the shelf break. The temperature front, defined by the 8 and 12°C isotherm, is ~15 km wide, and it inclines offshore at a slope of ~2–3 ($\times 10^{-3}$). The salinity distribution is identical to the temperature distribution, as both temperature and salinity are conserved. On the other hand, because the low temperature compensates for the low salinity, the density gradient across the outer shelf is more gradual with a width of ~40 km (Fig. 7b). The steady-state temperature (salinity) and density structure are remarkably similar to the conceptual model derived from the observations (see Fig. 14 in Allen et al., 1983).

The cross-shore circulation (Fig. 7b) indicates an offshore flow at the surface, sinking at the seaward side of the front, a strong return flow near the bottom and rising at the shoreward side of the front. The maximum cross-shore velocity is ~0.5 cm s^{-1} and the maximum vertical velocity is ~0.5 × 10^{-3} cm s^{-1}. The cross-shore circulation is embedded in the density front, and therefore, its horizontal extent is much wider than the temperature–salinity front. In fact, the temperature–salinity front is located entirely in the convergence zone.

The alongshore velocity (Fig. 7c) has a jet-like feature centered near the shelf break; the maximum southward flow is ~10 cm s^{-1} at the surface. Due to large friction the jet vanishes near the bottom. The total southward transport is 1.2 × 10^5 m^3 s^{-1}. For comparison, Beardsley et al. (1976) found that the total wintertime alongshore transport across the New England shelf–slope was about 1.7 × 10^5 m^3 s^{-1} (5300 km^3 yr^{-1}).

5. Conclusion

A density front is maintained by the strong surface convergence along the boundary between two water masses. For the nonrotating case, the propagation of the front is governed by a balance between buoyancy and inertia forces. The viscous drag slows the frontal motion, and a sloping bottom restrains the up-slope propagation of a bottom front. With Earth rotation included, a stationary front is formed for which the buoyancy force is balanced by the Coriolis force. A cross-frontal circulation is induced by the vertical viscosity.

The cause for seasonal mean circulation on continental shelves has always been an intriguing subject.
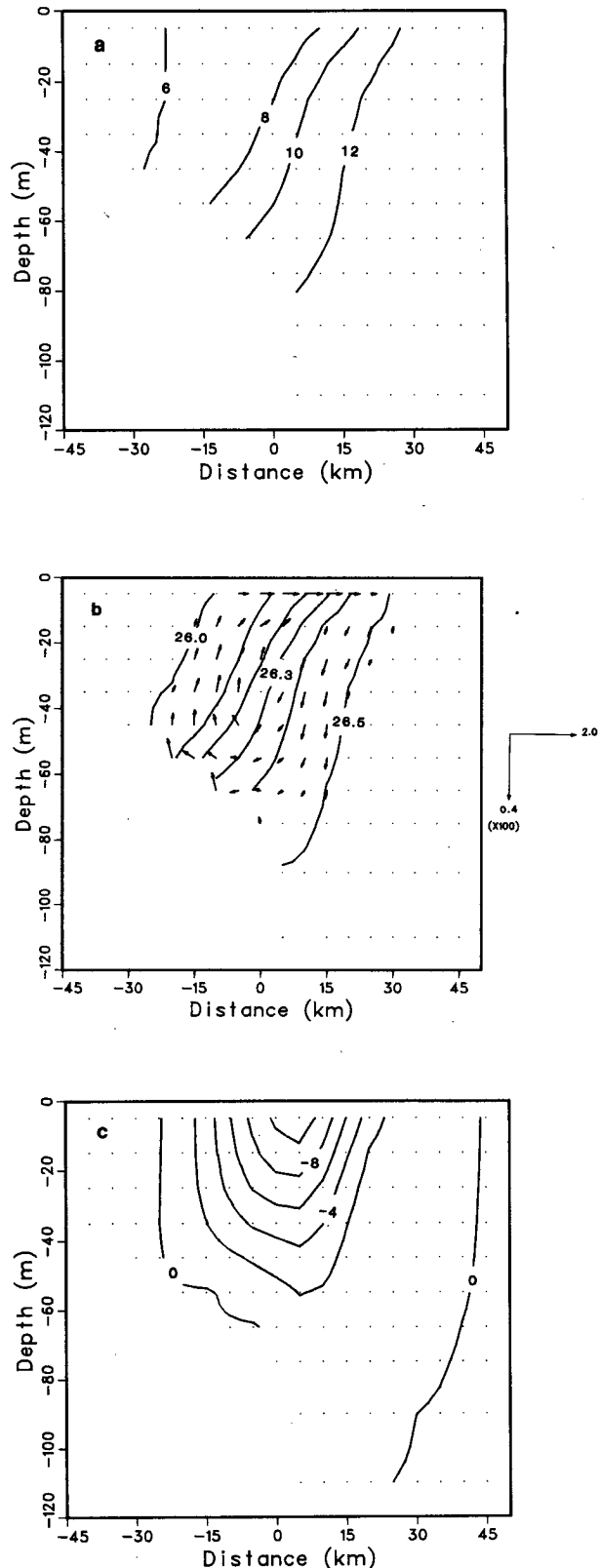

FIG. 7. As in Fig. 6 but for the New England Shelf: (a) temperature (deg), (b) the cross-shore circulation (cm s^{-1}) and density (in 0.01σ_t) and (c) the alongshore velocity (cm s^{-1}).

For example, there have been suggestions that the clockwise gyre circulation around the Georges Bank is driven by tidal rectification (Loder, 1980) and that the southwestward flow on the Middle Atlantic Bight is driven by an alongshelf pressure gradient (Csanady, 1978a). Our shelf–slope front simulation indicates that the density difference between the shelf and slope water will drive a substantial mean flow comparable to the observed transport. Thus, the available potential energy, derived from river runoff and wind and tidal mixing, also appears to be a major source for maintaining the mean flow on continental shelves.

REFERENCES

Allen, J. S., R. C. Beardsley, J. O. Blanton, W. C. Boicourt, B. Butman, L. K. Coachman, A. Huyer, T. H. Kinder, T. C. Royer, J. D. Schumacher, R. L. Smith, W. Sturges and C. D. Winant, 1983: Physical oceanography of Continental shelves. *Rev. Geophys. Space Phys.*, **21**, 1149–1181.

Beardsley, R. C., W. C. Boicourt and D. V. Hansen, 1976: Physical oceanography of the Middle Atlantic Bight. *Middle Atlantic Continental Shelf and the New York Bight.* M. G. Gross, Ed., Amer. Soc. Limnol. Oceanogr., Special Symposia, **2**, 20–34.

Csanady, G. T., 1971: On the equilibrium shape of the thermocline in the shore zone. *J. Phys. Oceanogr.*, **1**, 263–270.

——, 1978a: The arrested topographic wave. *J. Phys. Oceanogr.*, **8**, 47–62.

——, 1978b: Wind effects on surface to bottom fronts. *J. Geophys. Res.*, **83**, 4633–4640.

Garvine, R. W., and J. D. Monk, 1974: Frontal structure of a river plume. *J. Geophys. Res.*, **79**, 2251–2259.

Hamilton, P., and M. Rattray, 1978: A numerical model of the depth-dependent wind-driven upwelling circulation on a continental shelf. *J. Phys. Oceanogr.*, **8**, 437–457.

Hsueh, Y., and B. Cushman-Roisin, 1983: On the formulation of surface to bottom fronts over steep topography. *J. Geophys. Res.*, **88**, 743–750.

Huppert, H., 1982: The propagation of two-dimensional and axisymmetric viscous gravity currents over a rigid horizontal surface. *J. Fluid Mech.*, **121**, 43–58.

James, I. D., 1978: A note on the circulation induced by a shallow-sea front. *Estuarine Coastal Mar. Sci.*, **7**, 197–202.

Kao, T. W., 1981: The dynamics of oceanic fronts. Part II: Shelf water structure due to freshwater discharge. *J. Phys. Oceanogr.*, **11**, 1215–1223.

——, C. Park and H-P. Pao, 1977: Buoyant surface discharge and small-scale oceanic fronts: A numerical study. *J. Geophys. Res.*, **82**, 1747–1752.

Loder, J., 1980: Topographic rectification of tidal currents on the side of Georges Bank. *J. Phys. Oceanogr.*, **10**, 1399–1416.

Mamayev, O. I., 1975: *Temperature-Salinity Analysis of World Ocean Waters.* Elsevier.

Muench, R. D., 1983: Mesoscale oceanographic features associated with the central Bering Sea ice edge: February–March 1981. *J. Geophys. Res.*, **88**, 2715–2722.

Ou, H. W., 1983: Some two-layer models of the shelf–slope front: geostrophic adjustment and its maintenance. *J. Phys. Oceanogr.*, **13**, 1798–1808.

Sick, L. V., C. C. Johnson and R. Engel, 1978: Trace metal enhancement in the biotic and abiotic components of an estuarine tidal front. *J. Geophys. Res.*, **83**, 4659–4667.

Simpson, J. H., C. M. Allen and N. C. G. Morris, 1978: Fronts on the continental shelf. *J. Geophys. Res.*, **83**, 4607–4614.

Wang, D-P., 1982: Development of a three-dimensional limited-area (island) shelf circulation model. *J. Phys. Oceanogr.*, **12**, 605–617.

——, and D. W. Kravitz, 1980: A semi-implicit two-dimensional model of estuarine circulation. *J. Phys. Oceanogr.*, **10**, 441–454.